Materials Transactions, Vol. 50, No. 1 (2009) pp. 204 to 209

EXPRESS REGULAR ARTICLE

FeSiBPCu Nanocrystalline Soft Magnetic Alloys with High B_s of 1.9 Tesla Produced by Crystallizing Hetero-Amorphous Phase

Akihiro Makino, He Men*, Takeshi Kubota, Kunio Yubuta and Akihisa Inoue

Institute for Materials Research, Tohoku University, Sendai 980-8577, Japan

Technically important nanocrystalline soft magnetic alloys and their derivatives always include metal elements such as Nb, Zr, Mo, etc. and/or Cu to realize the nanostructure, which results in a remarkable decrease of saturation magnetic flux density (B_s) and a significant increase in material cost. With the aim to solve the serious problem, we successfully developed new FeSiBPCu nanocrystalline soft magnetic alloys. The melt-spun $Fe_{83.3-84.3}Si_4B_8P_{3-4}Cu_{0.7}$ (at%) alloys have heterogeneous amorphous structures including a large amount of α-Fe clusters, 2–3 nm in size, due to the unusual effect of the simultaneous addition of the proper amounts of P and Cu. The hetero-amorphous alloys exhibit higher B_s of about 1.67 T than the representative amorphous and the nanocrystalline alloys, and the low coercivity (H_c) of 5–10 Am^{-1}. A homogeneous nanocrystalline structure composed of small α-Fe grains with a size of about 10 nm can be realized by crystallizing the hetero-amorphous alloys. The nanocrystalline alloys show extremely high B_s of 1.88–1.94 T almost comparable to the commercial Fe-3.5 mass%Si crystalline soft magnetic alloys, and low H_c of 7–10 Am^{-1} due to the simultaneous realization of the homogeneous nanocrystalline structure and small magnetostriction of 2–3 $\times 10^{-6}$. In addition, the alloys have a large economical advantage of lower material cost and better productivity than the ordinary soft magnetic nanocrystalline alloys now in practical use. [doi:10.2320/matertrans.MER2008306]

(Received September 2, 2008; Accepted November 5, 2008; Published December 17, 2008)

Keywords: *soft magnetic material, high saturation magnetic flux density, amorphous alloy, nanocrystalline alloy*

1. Introductions

Nanocrystalline soft magnetic alloys[1–3] produced by crystallizing amorphous phases attracted great attention due to their excellent soft magnetic properties and rather high magnetizations. The developed nanocrystalline soft magnetic alloys and their derivatives always include a large amount of metal elements such as Nb, Zr, Mo, etc. and/or Cu to realize the nanocrystallized structure.[4–8] It is well-known that the uniform nanocrystalline structure with excellent magnetic softness can be obtained by an amorphous precursor including some chemical or topological heterogeneities induced by the above-mentioned metal elements.[9,10] During heating, an apparent short-medium range ordering[11] or a nanoscale phase separation[12] in the amorphous matrix raises from the heterogeneity, which acts as the nucleation site for the primary crystal and leads to the refinement of the grains. Thus, the precursor for nanocrystallized structure is needed to be an amorphous phase essentially including the metal elements, however, which cause a remarkable decrease of the saturation magnetic flux density (B_s)[13] and a significant increase of the material cost. Considering current energy problems, higher B_s accompanied with excellent magnetic softness is strongly required for the magnetic materials used in electrical power supplies.

We developed new $Fe_{83.3-84.3}Si_4B_8P_{3-4}Cu_{0.7}$ (at%) nanocrystalline soft magnetic alloys with much higher B_s of around 1.9 T than those of the representative amorphous, the ordinary[1–3,5,8] and the recently reported[14,15] nanocrystalline alloys, almost comparable to Fe-3.5 mass%Si crystalline alloys[16] now in practical use.

2. Experimental Procedure

FeSiBPCu alloy ingots were prepared by induction-melting mixtures of Fe (99.98 mass%), Si (99.998 mass%), B (99.5 mass%), Cu (99.99 mass%) and premelted Fe-P (99.9 mass%) in a high purity Argon atmosphere. $Fe_{78}Si_9B_{13}$ alloy ingot was also prepared by the same method for comparison. A single-roller melt-spinning method in air was used to produce the rapidly solidified tapes with about 1–3 mm in width and approximately 20 μm in thickness. The alloy compositions are nominally expressed since the difference between nominal and chemical analyzed composition was negligibly small. The structure was identified by X-ray diffractometry (XRD) and transmission electron microscopy (TEM). The mean grain size of the α-Fe phase was estimated by using Scherrer's equation from the full width at half maximum of the bcc(110) reflection peak from for the specimens. Thermal property of melt-spun alloys was evaluated with a differential scanning calorimeter (DSC) at a heating rate of 0.67°C/s under an Argon flow. The melt-spun specimens were subjected to annealing for 600 seconds at various temperatures in a vacuum atmosphere under the non-magnetic field. Saturation magnetization (J_s) and coercivity (H_c) under a maximum applied field of 800 kAm^{-1} and 2 kAm^{-1} were measured by a vibrating sample magnetometer (VSM) and a dc B-H loop tracer, respectively. Effective permeability (μ_e) at 1 kHz and core loss (W) at 50 Hz for were measured with a vector impedance analyzer under a field of 0.4 Am^{-1} and an ac B-H analyzer operated under sinusoidal input voltage, respectively, by using the wounded toroidal cores with a diameter of about 20 mm. The W and μ_e should be inferior to those measured by using a single sheet and a ring sample. Magnetostriction was measured in an applied field up to 800 kAm^{-1} by using a strain gauge. Density was measured by the Archimedean method with n-tridecane.

3. Results and Discussion

3.1 Microstructure of as-quenched alloys

Figure 1 shows the dependence of α-Fe grain size on the substitutional amounts of P for B and Cu for Fe in an as-

*Graduate Student, Tohoku University

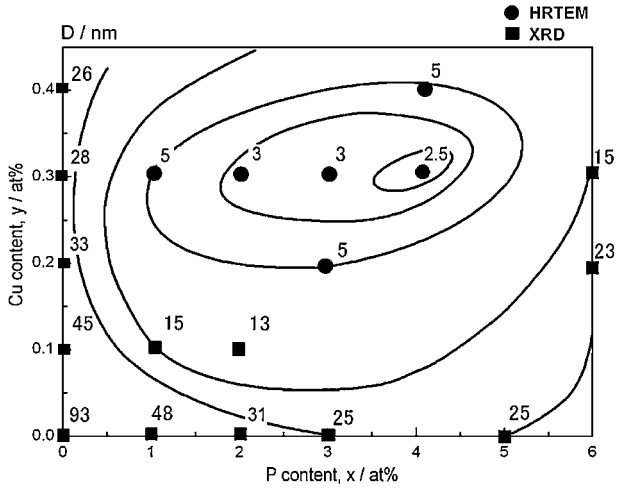

Fig. 1 Dependence of α-Fe grain size on substitutional amounts of P for B and Cu for Fe in $Fe_{82-y}Si_9B_{9-x}P_xCu_y$ in an as-quenched state.

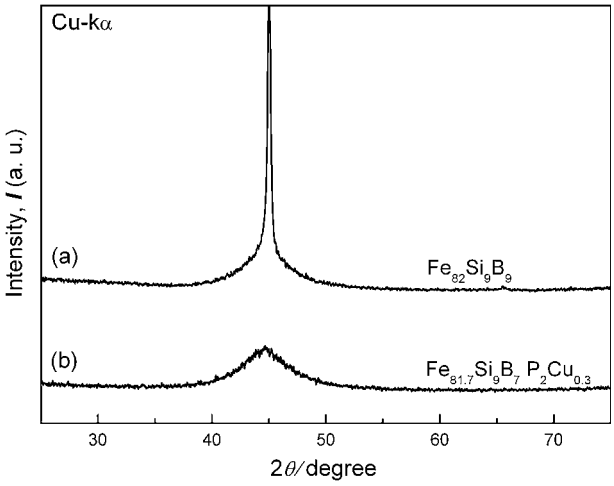

Fig. 2 XRD profiles for as-quenched (a) $Fe_{82}Si_9B_9$ and (b) $Fe_{81.7}Si_9B_7P_2Cu_{0.3}$ alloys.

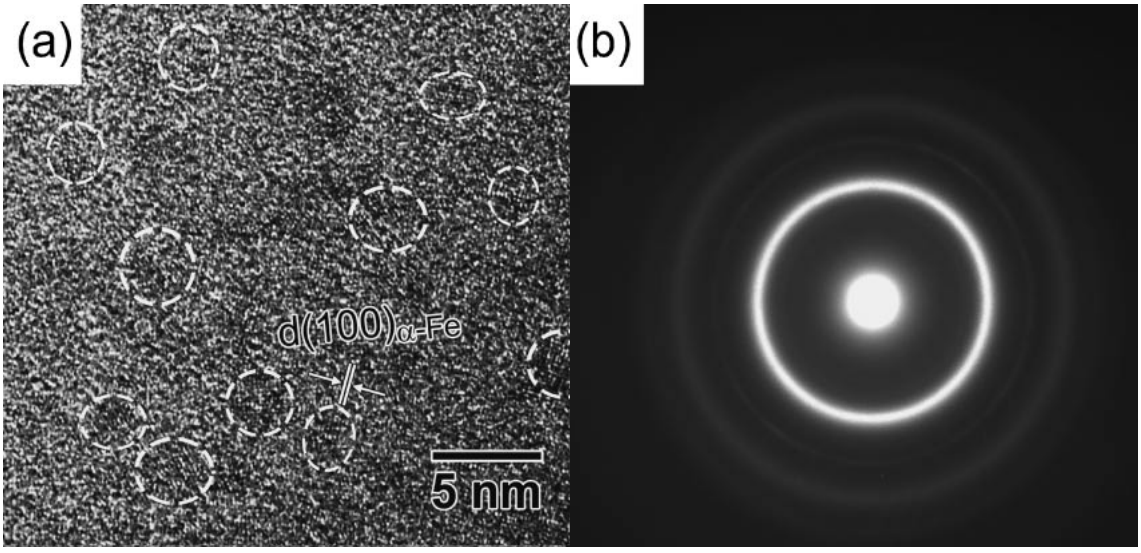

Fig. 3 (a) HRTEM image and (b) SAED pattern for as-quenched $Fe_{81.7}Si_9B_7P_2Cu_{0.3}$ alloy.

quenched $Fe_{82}Si_9B_9$ alloy with higher Fe content than the limit of about 80% for the formation of a single amorphous structure. The grain size is estimated from a sharp diffraction peak at about 45° corresponding to α-Fe phase in the XRD profiles or the high resolution TEM (HRTEM) images. The alloy without P and Cu has the largest α-Fe grains with the size of 93 nm estimated from XRD profile, shown in Fig. 2(a). The grain size decreases with the P and/or Cu addition, and reaches to the minimum values of around 3 nm smaller for the alloys simultaneously containing 2–4 at%P and 0.3%Cu. The grain size for the alloys with the proper amounts of P and Cu is much smaller than that for the recently reported the FeCuB(Si) alloys.[14] The XRD profile, the HRTEM image and the selected area electron diffraction (SAED) pattern of the as-quenched $Fe_{81.7}Si_9B_7P_2Cu_{0.3}$ alloy are shown in Fig. 2(b), Fig. 3(a) and (b), respectively. The SAED pattern shows diffused diffraction rings and no spots corresponding to any crystalline phase in agreement with the XRD results shown in Fig. 2(b). However, the HRTEM image reveals that the as-quenched structure of the alloy is not fully amorphous in disagreement with the XRD and the SAED patterns, but consists of an extremely small crystalline-like phase with about 3 nm or smaller in diameter, randomly dispersed within the amorphous matrix. Judging from the lattice fringes as indicated by white bars in Fig. 3(a), corresponding to the bcc (110) plane distance of α-Fe crystalline, the phase is completely revealed to be α-Fe crystal. It is understandable that the XRD and the SAED patterns are not able to reveal the existence of the nanocrystals due to their very small size and low volume fraction.[17] Therefore, we can notice that the coarse α-Fe grains formed within the as-quenched amorphous matrix of $Fe_{82}Si_9B_9$ alloy change to the nano-sized α-Fe phase with 3 nm or smaller in size by the simultaneous substitution of 2–4%P for B and 0.3%Cu for Fe. With deviation from these compositions with the P and the Cu contents, the grain size rapidly increases.

We discuss on the origin of the remarkable effect of the simultaneous addition of P and Cu on the refinement of the α-Fe crystals formed in the amorphous matrix of the alloys with

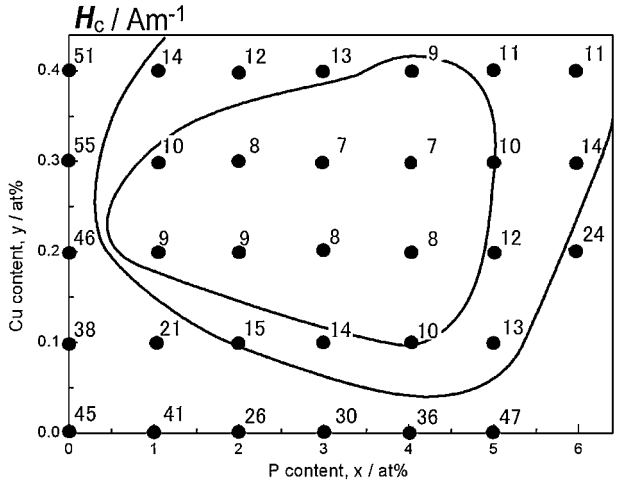

Fig. 4 Compositional dependence of H_c on P and Cu contents for as-quenched $Fe_{82-y}Si_9B_{9-x}P_xCu_y$ (x: 0–6, y: 0–0.4) alloys.

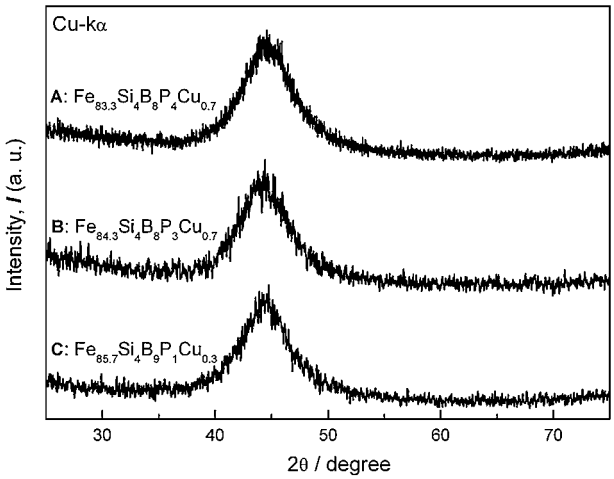

Fig. 5 XRD profiles for as-quenched $Fe_{83.3}Si_4B_8P_4Cu_{0.7}$ (A), $Fe_{84.3}Si_4B_8P_3Cu_{0.7}$ (B) and $Fe_{85.7}Si_4B_9P_1Cu_{0.3}$ (C) alloys.

higher Fe content than the limit for formation of a single amorphous phase. Taking account of the result that the effect is observed only for the simultaneous addition of the proper amounts of P and Cu, the mixing enthalpy (ΔH)[18] between the constituent elements is considered. It is noted that ΔH is positive (+13 kJ/mol) between Fe and Cu and negative (−9 kJ/mol) between Cu and P, suggesting that there is a repulsive and an attractive interactions existing between Fe and Cu, and Cu and P atoms, respectively. Therefore, during melt-spinning, an extremely small region including enriched Cu and P elements could separate from the Fe-Si-B-(P) amorphous phase and possibly act as the nucleation sites for α-Fe clusters, which should result in the refinement of the grains. The number and the size of the Cu- and P-rich region possibly change with the amounts of P and Cu. The simultaneous addition of 2–4%P and around 0.3%Cu might realize the smallest size and the largest number of the region, which is considered to be most suitable condition for decreasing the α-Fe precipitates.

Figure 4 shows the compositional dependence of H_c on P and Cu contents for the as-quenched $Fe_{82-y}Si_9B_{9-x}P_xCu_y$ (x: 0–6, y: 0–0.4) alloys. The dependence coincides with the change in the α-Fe grain size with P and Cu addition shown in Fig. 1. The alloy without the addition of P and Cu has the largest H_c of about 45 Am^{-1} responsible to the coarse α-Fe grains. The H_c decreases with decreasing the grain size, and reaches the minimum value of 7–8 Am^{-1} for the hetero-amorphous alloys with 2–4%P and around 0.3%Cu.

The similar effect of the simultaneous addition of P and Cu was observed for the alloys with higher Fe content up to 85.7%. Figure 5 shows the XRD profiles for $Fe_{83.3}Si_4B_8P_4Cu_{0.7}$ ("A" alloy), $Fe_{84.3}Si_4B_8P_3Cu_{0.7}$ ("B" alloy) and $Fe_{85.7}Si_4B_9P_1Cu_{0.3}$ ("C" alloy), indicating an amorphous structure with small H_c of 7, 8 and 11 Am^{-1}, respectively. Whereas, the HRTEM observation revealed that the alloys have an as-quenched hetero-amorphous structure with a large amount of α-Fe clusters, as shown in Fig. 6 for "A" alloy as an example. The hetero-amorphous alloys have higher B_s of about 1.67 T than the FeSiB amorphous alloy now in practical use. Moreover, all the alloys shown in Fig. 1 and hetero-amorphous "A", "B" and "C" alloys are confirmed to be completely ductile in three-point bending test, which is important for applications.

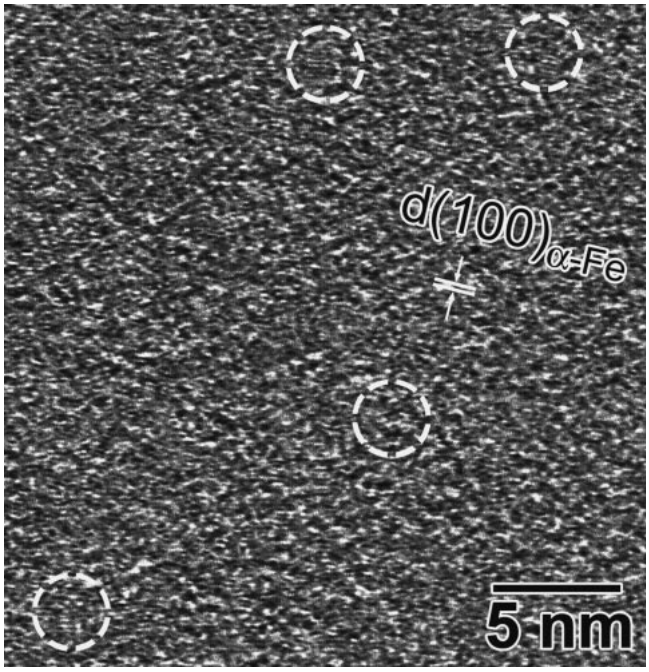

Fig. 6 HRTEM image of as-quenched $Fe_{83.3}Si_4B_8P_4Cu_{0.7}$ alloy.

3.2 Microstructure and magnetic properties of crystallized alloys from hetero-amorphous phase

Crystallization behavior was examined by DSC for the hetero-amorphous "A" and "B" alloys, shown in Fig. 7. The alloys crystallize through two exothermic peaks and large temperature intervals of 168°C and 135°C between each one, respectively. It was confirmed by XRD that the first and the second peaks on the curves result from the phase transition from the amorphous to α-Fe and then to some compounds, respectively. It has been already reported in the representative nanocrystalline soft magnetic alloys "Nanoperm"[2,19] that the amorphous precursor with a large temperature

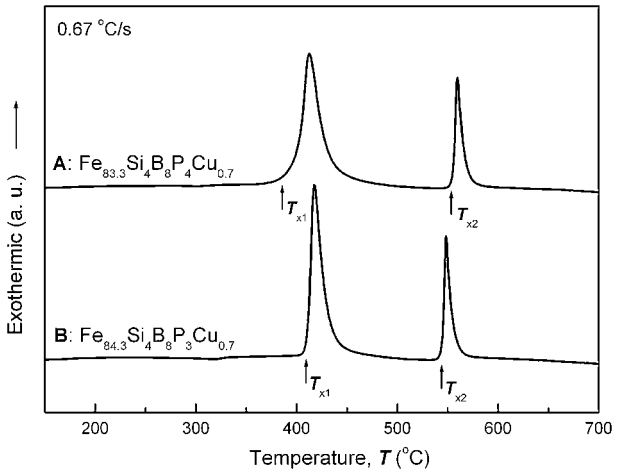

Fig. 7 DSC curves for as-quenched $Fe_{83.3}Si_4B_8P_4Cu_{0.7}$ (A) and $Fe_{84.3}Si_4B_8P_3Cu_{0.7}$ (B) alloys.

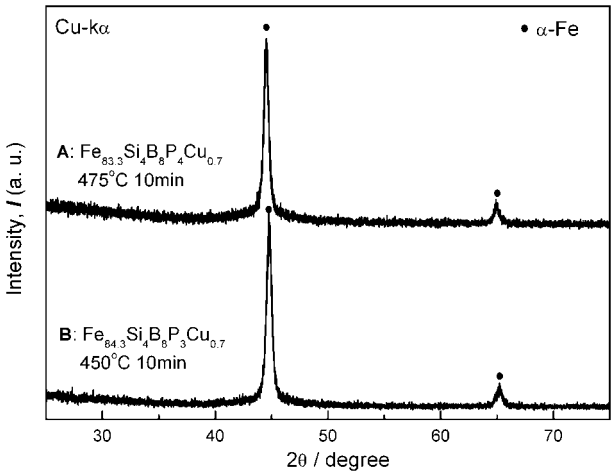

Fig. 8 XRD profiles for $Fe_{83.3}Si_4B_8P_4Cu_{0.7}$ (A) and $Fe_{84.3}Si_4B_8P_3Cu_{0.7}$ (B) alloys.

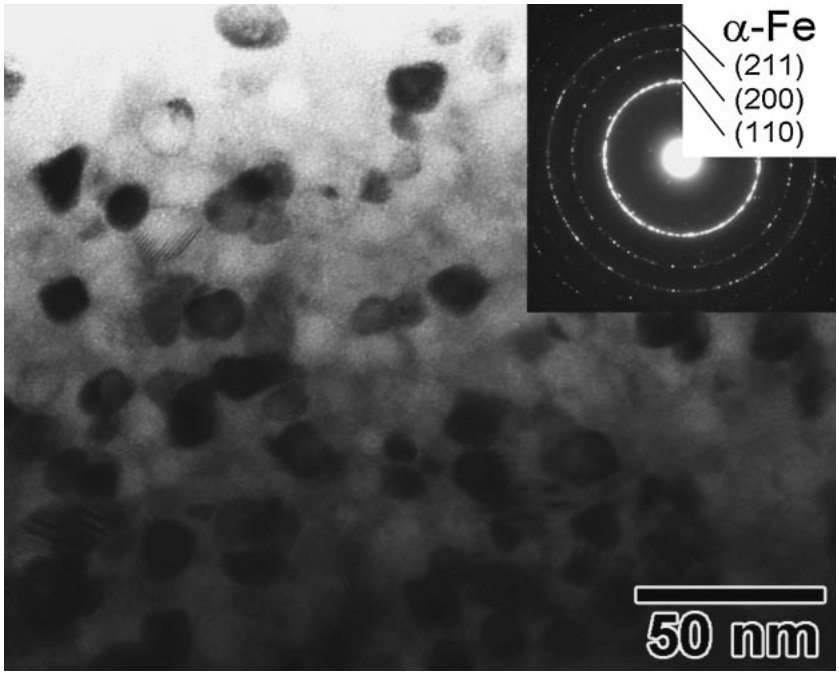

Fig. 9 Bright field image and SAED patterns of nanocrystalline $Fe_{83.3}Si_4B_8P_4Cu_{0.7}$ alloy.

interval can change to a uniform nanocrystalline structure without any compounds with large magnetocrystalline anisotropy by annealing within the temperature range between the two peaks.

Figure 8 shows the XRD profiles for "A" and "B" alloys crystallized at 475°C and 450°C, respectively, between the temperatures of the two peaks on the DSC curves. The structures were found to consist of α-Fe phase, whose grain sizes were estimated to be 11 nm and 17 nm for "A" and "B" alloys, respectively. The SAED profile and the TEM image of nanocrystalline "A" alloy are shown in Fig. 9. A uniform nanocrystalline structure with the grain size of approximately 10 nm, which is in almost agreement with the estimated value from the XRD profile, is successfully formed presumably because the cluster formed at an as-quenched state could act as the nucleation site for the α-Fe grains during the crystallization. The structure is very similar to the previously developed representative nanocrystallized alloys with excellent magnetic softness[1,2,20,21] in spite of not-containing a large amount of the metal elements.

Figure 10 shows the hysteresis loop the nanocrystalline "A" alloy. The alloy shows the extremely high $\boldsymbol{B}_s$ of 1.88 T due to the high Fe content and almost not-containing any metal elements except for Fe. The $\boldsymbol{B}_s$ is higher than those of the amorphous and the previously reported nanocrystalline alloys,[1–3,13,15] and slightly lower than the Fe-3.5 mass%Si crystalline soft magnetic alloys.[16] "A" alloy also exhibits the low $\boldsymbol{H}_c$ of 7 Am^{-1} and the high $\boldsymbol{\mu}_e$ of 25,000 due to the simultaneous realization of the homogeneous nanocrystalline structure and the much smaller magnetostriction ($\boldsymbol{\lambda}$) of $+2 \times 10^{-6}$ than that of $+27 \times 10^{-6}$ of $Fe_{78}Si_9B_{13}$ amorphous alloy.

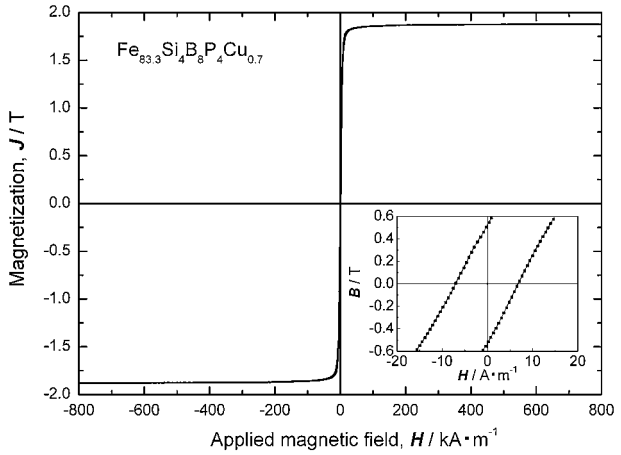

Fig. 10 Hysteresis loop for the nanocrystalline $Fe_{83.3}Si_4B_8P_4Cu_{0.7}$ alloy measured by a VSM. Insert shows enlarge part of near zero field measured by a dc B-H tracer.

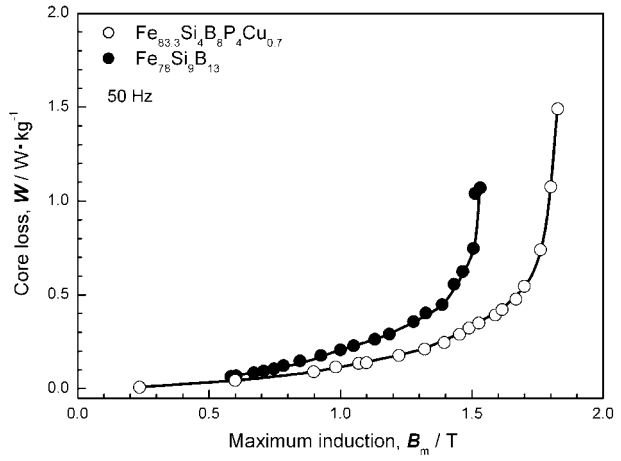

Fig. 11 Core loss ($\boldsymbol{W}$) of nanocrystalline $Fe_{83.3}Si_4B_8P_4Cu_{0.7}$ alloy as a function of maximum magnetic flux density ($\boldsymbol{B}_m$). The data of $Fe_{78}Si_9B_{13}$ amorphous alloy annealed at 380°C for 120 min are also shown for comparison.

Core loss ($\boldsymbol{W}$) is important for the materials in power devices. Figure 11 shows the $\boldsymbol{W}$ at 50 Hz of the nanocrystalline "A" alloy as a function of maximum magnetic flux density ($\boldsymbol{B}_m$), in comparison with the data of the optimal annealed $Fe_{78}Si_9B_{13}$ amorphous alloy. Comparing to the commercial non-oriented and the oriented Fe-3 mass%Si, $\boldsymbol{W}$ at $\boldsymbol{B}_m$ of 1 T for the nanocrystalline alloy is much smaller than those measured by using punched ring samples for the Fe-Si alloys.[22] Although the $\boldsymbol{W}$ of the nanocrystalline and the amorphous alloys increase with increasing $\boldsymbol{B}_m$, the nanocrystalline alloy exhibits the superior $\boldsymbol{W}$ to the amorphous alloy over the whole $\boldsymbol{B}_m$ range. The rapid increase of $\boldsymbol{W}$ takes place at higher $\boldsymbol{B}_m$ of 1.7 T for the nanocrystalline alloy than that of 1.4 T for the amorphous alloy. Here, the very low $\boldsymbol{W}$ in the $\boldsymbol{B}_m$ range up to 1.7 T of the nanocrystalline alloy should be an outstanding feature never seen in the other soft magnetic materials.

The nanocrystalline "B" alloy with higher Fe content have a high $\boldsymbol{B}_s$ of 1.94 T comparable to Fe-3.5 mass%Si alloy, and accompanied with low $\boldsymbol{H}_c$ of 10 Am^{-1} due to small $\boldsymbol{\lambda}$ of $+3 \times 10^{-6}$.

These nanocrystalline alloys should make a contribution to energy saving though their low core losses and improve the conversation of earth resources. In addition, the alloys have a large economical advantage of low material cost and good productivity because of not-containing expensive and easily oxidized metal elements which has been considered to be essential for the nanocrystalline soft magnetic alloys.

4. Conclusions

Structure and magnetic properties of as-quenched and crystallized Fe-rich FeSiBPCu alloys were studied. The uniform nanocrystalline structure composed of α-Fe grains is found to be realized by annealing the hetero-amorphous structure with α-Fe clusters formed by an unusual effect of the simultaneous addition of P and Cu. The conclusions obtained are summarized as follows.

(1) The simultaneous substitution of 2–4%P for B and 0.3%Cu for Fe significantly and drastically decreases the size of α-Fe grains within the as-quenched amorphous matrix of an as-quenched $Fe_{82}Si_9B_9$ alloy from 93 nm to 3 nm or smaller. That refinement effect was also observed for the alloys with higher Fe content up to 85.7%.

(2) The melt-spun $Fe_{83.3-84.3}Si_4B_8P_{3-4}Cu_{0.7}$ alloys with heterogeneous amorphous structures including a large number of α-Fe clusters exhibit higher $\boldsymbol{B}_s$ of about 1.67 T than the representative $Fe_{78}Si_9B_{13}$ amorphous alloy, and the low $\boldsymbol{H}_c$ of 5–10 Am^{-1}.

(3) The uniform nanocrystallized structures from the hetero-amorphous alloys consist of small α-Fe grains with about 10 nm evaluated from the TEM image and 17 nm estimated from the XRD profile in size for $Fe_{83.3}Si_4B_8P_4Cu_{0.7}$ and $Fe_{84.3}Si_4B_8P_3Cu_{0.7}$, respectively. With the structural change from the amorphous to the nanocrystalline structure, the $\boldsymbol{B}_s$ rapidly increases from 1.67 T to 1.88–1.94 T.

(4) The $\boldsymbol{B}_s$ of the nanocrystalline alloys is considerably higher than those of any soft magnetic amorphous and nanocrystalline alloys previously reported.

(5) The $Fe_{83.3}Si_4B_8P_4Cu_{0.7}$ nanocrystalline alloy exhibits excellent magnetic softness, $\boldsymbol{H}_c$ of 7 Am^{-1} and $\boldsymbol{\mu}_e$ of 25,000 at 1 kHz, due to the simultaneous realization of the uniform nanostructure composed by small α-Fe grains with about 10 nm in size and a small magnetostriction of 2×10^{-6}.

(6) The $Fe_{83.3}Si_4B_8P_4Cu_{0.7}$ nanocrystalline alloy exhibits the extremely lower $\boldsymbol{W}$ over the whole $\boldsymbol{B}_m$ range than the $Fe_{78}Si_9B_{13}$ amorphous alloy. The rapid increase of $\boldsymbol{W}$ takes place at higher $\boldsymbol{B}_m$ of 1.7 T for the nanocrystalline alloy than that of 1.4 T for the amorphous alloy.

REFERENCES

1) Y. Yoshizawa, S. Oguma and K. Yamauchi: J. Appl. Phys. **64** (1988) 6044–6046.
2) K. Suzuki, A. Makino, N. Kataoka, A. Inoue and T. Masumoto: Mater. Trans. JIM **32** (1991) 93–102.
3) M. A. Willard, D. E. Laughlin, M. E. McHenry, D. Thoma, K. Sickafus, J. O. Cross and V. G. Harris: J. Appl. Phys. **84** (1998) 6773–6777.

4) Y. Yoshizawa and K. Yamauchi: Mater. Trans. JIM **31** (1990) 307–314.
5) A. Makino, T. Hatanai, Y. Naitoh, T. Bitoh, A. Inoue and T. Masumoto: IEEE Trans. Magn. **33** (1997) 3797–3798.
6) A. Makino, A. Inoue and T. Masumoto: Mater. Trans. JIM **36** (1995) 924–938.
7) K. Suzuki, N. Kataoka, A. Inoue and A. Makino: Mater. Trans. JIM **31** (1990) 743–746.
8) K. Suzuki, A. Makino, A. Inoue and T. Masumoto: Sci. Rep. RITU A**39** (1994) 133–140.
9) J. D. Ayers, V. G. Harris, J. A. Sprague, W. T. Elam and H. N. Jones: Acta Mater. **46** (1998) 1861–1874.
10) Y. Zhang, K. Hono, A. Inoue, A. Makino and T. Sakurai: Acta Mater. **44** (1996) 1497–1510.
11) M. Nakamura, Y. Hirotsu, K. Anazawa, A. Makino and A. Inoue: Mater. Sci. Eng. A **179/180** (1994) 487–490.
12) M. Ohnuma, K. Hono, H. Onodera, J. S. Pedersen and S. Linderoth: NanoStructured Mater. **11** (1999) 693–696.
13) M. E. McHenry, M. A. Willard and D. E. Laughlin: Prog. Mater. Sci. **44** (1999) 291–433.
14) M. Ohta and Y. Yoshizawa: Jpn. J. Appl. Phys. **46** (2007) L477–L479.
15) M. Ohta and Y. Yoshizawa: Appl. Phys. Lett. **91** (2007) 062517 (3pages).
16) A. Makino, K. Suzuki, A. Inoue and T. Masumoto: Mater. Trans. JIM **32** (1991) 551–556.
17) K. Hono, D. H. Ping, M. Ohnuma and H. Onodera: Acta Mater. **47** (1999) 997–1006.
18) A. Takeuchi and A. Inoue: Mater. Trans. **46** (2005) 2817–2829.
19) K. Suzuki, M. Kikuchi, A. Makino, A. Inoue and T. Masumoto: Mater. Trans. JIM **32** (1991) 961–968.
20) A. Makino, T. Bitoh, A. Inoue and T. Masumoto: Scr. Mater. **48** (2003) 869–874.
21) A. Makino, M. Bingo, T. Teruo, K. Yubuta and A. Inoue: J. Appl. Phys. **101** (2007) 09N117 (3pages).
22) Y. Takada, M. Abe, S. Masuda and J. Inagaki: J. Appl. Phys. **64** (1988) 5367–5369.